High-speed, low-photodamage nonlinear imaging using passive pulse splitters

Na Ji, Jeffrey C Magee & Eric Betzig

Supplementary figures and text:

Supplementary Figure 1 A monolithic 10x pulse splitter with interfacial coating of variable reflectivity.

Supplementary Figure 2 A monolithic 16x pulse splitter with 50% and 100% interfacial coating.

Supplementary Figure 3 Optical layouts for five different pulse splitting geometries.

Supplementary Figure 4 Temporal sequences of sub-pulses generated by pulse splitters in Supplementary Figure 3.

Supplementary Figure 5 Unnormalized photobleaching curves of GFP-labeled *C. elegans.*

Supplementary Figure 6 Ca^{2+} transient traces obtained with and without pulse splitting.

Supplementary Methods

Supplementary Figure 1 A monolithic 10x pulse splitter with interfacial coating of variable reflectivity.

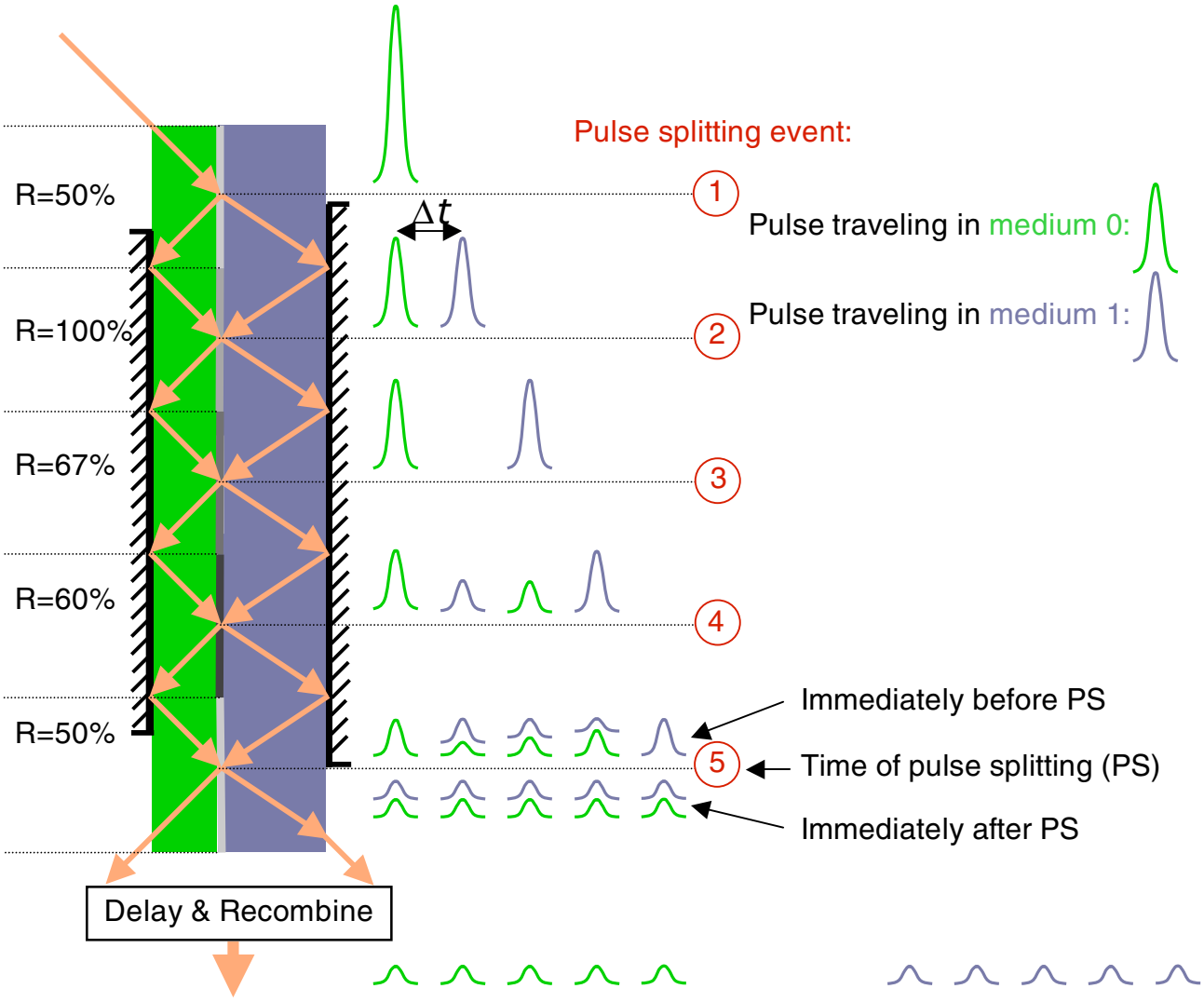

Supplementary Figure 1. Schematic outlining the generation of ten equal-energy sub-pulses from one input pulse, using a monolithic pulse splitter having variable reflectivity at the interface between two media. The reflectivity at each of the five interfacial pulse splitting locations is shown at left. The input pulse arrives from the left side of the splitter and the ten resulting sub-pulses exit as two trains of five pulses each from the exit ports of the splitter, after which they are time delayed relative to one another and finally recombined. All pulses, including intermediate ones, are color-coded according to the medium they are in immediately before each pulse splitting event, and are arranged according to their temporal sequence. t is the splitter-induced time delay, as defined in the main text.

Supplementary Figure 2 A monolithic 16x pulse splitter with 50% and 100% interfacial coating.

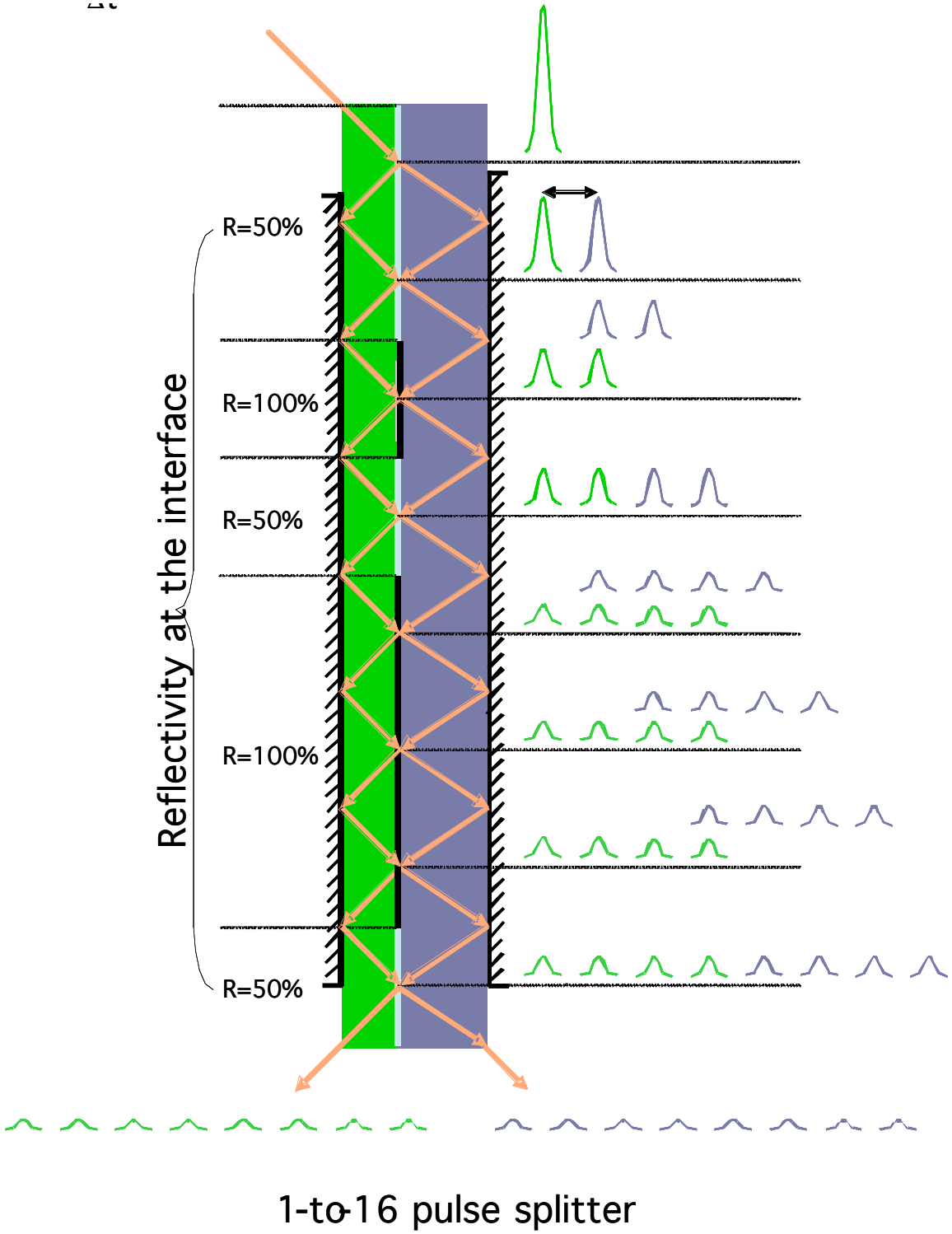

Supplementary Figure 2. Schematic outlining the generation of 16 equal-energy pulses from one input pulse, in a monolithic splitter requiring only interfacial coatings of 50% and 100% reflectivity. Details on the symbols can be found in the caption to **Supplementary Fig. 1**.

Supplementary Figure 3 Optical layouts for five different pulse splitting geometries.

a. 8x pulse splitter (37 ps minimal pulse delay)

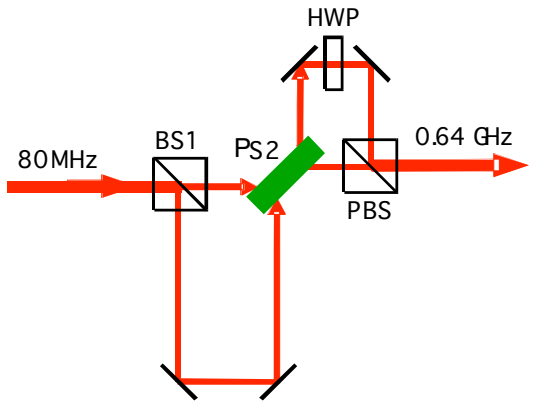

b. 8x pulse splitter (74 ps minimal pulse delay)

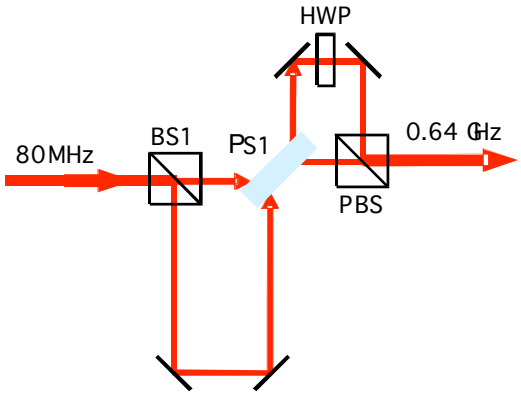

c. 8x pulse splitter (>1 ns minimal pulse delay)

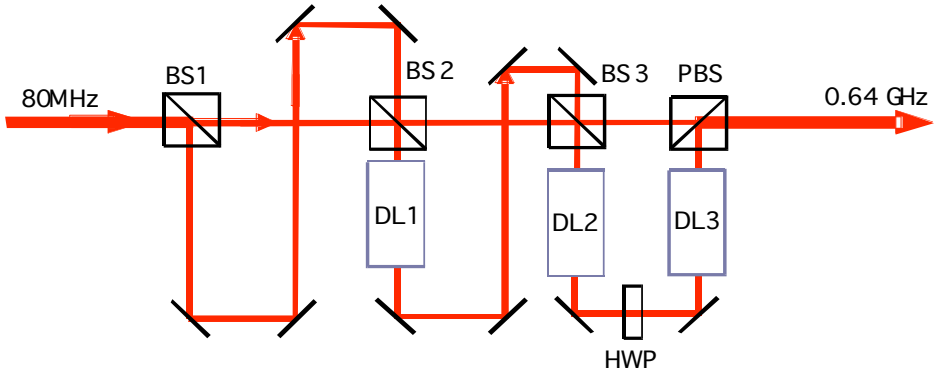

d. 64x pulse splitter (37 ps minimal pulse delay)

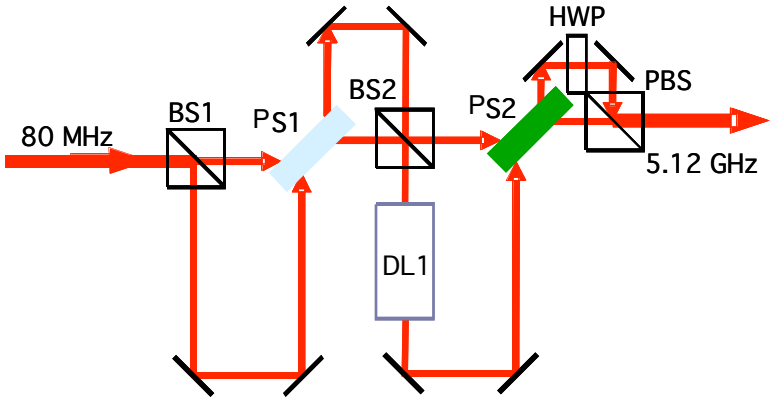

e. 128x pulse splitter (37 ps minimal pulse delay)

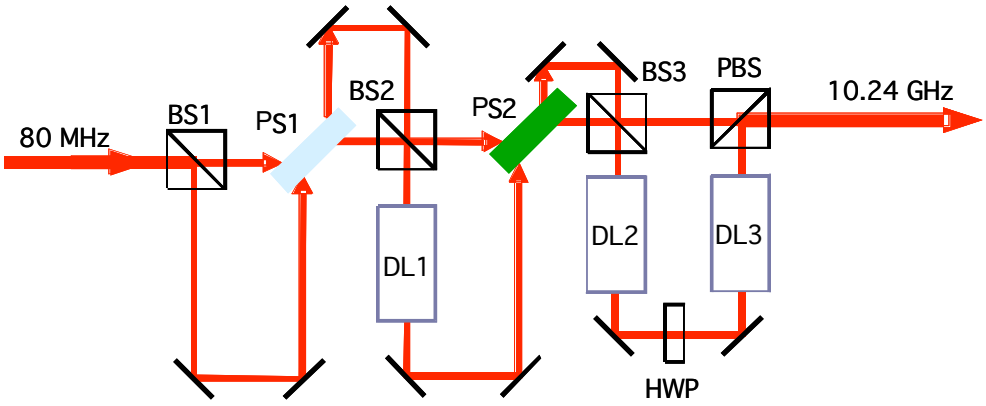

Supplementary Figure 3. Optical layouts for five different pulse splitting geometries described in the main text, characterized by their pulse splitting ratio and minimum pulse spacing t: (a) 8x splitting, t = 37 ps; (b) 8x splitting, t = 74 ps; (c) 8x splitting, t > 1 ns; (d) 64x splitting, t = 37 ps; (e) 128x splitting, t = 37 ps. In these layouts, blue pulse splitter PS1 creates a 74 ps delay between nearest pulses, while green pulse splitter PS2 creates a 37 ps delay. Other symbols were explained in the caption of **Fig. 2** of the main text. The power throughputs are ~90%, 50%, and 35% for 8x, 64x, and 128x pulse splitters, respectively. Power throughput may be significantly improved with next generation monolithic beam splitters, as described in **Supplementary Figs. 1** and **2**.

Supplementary Figure 4 Temporal sequences of sub-pulses generated by pulse splitters in **Supplementary Fig. 3**.

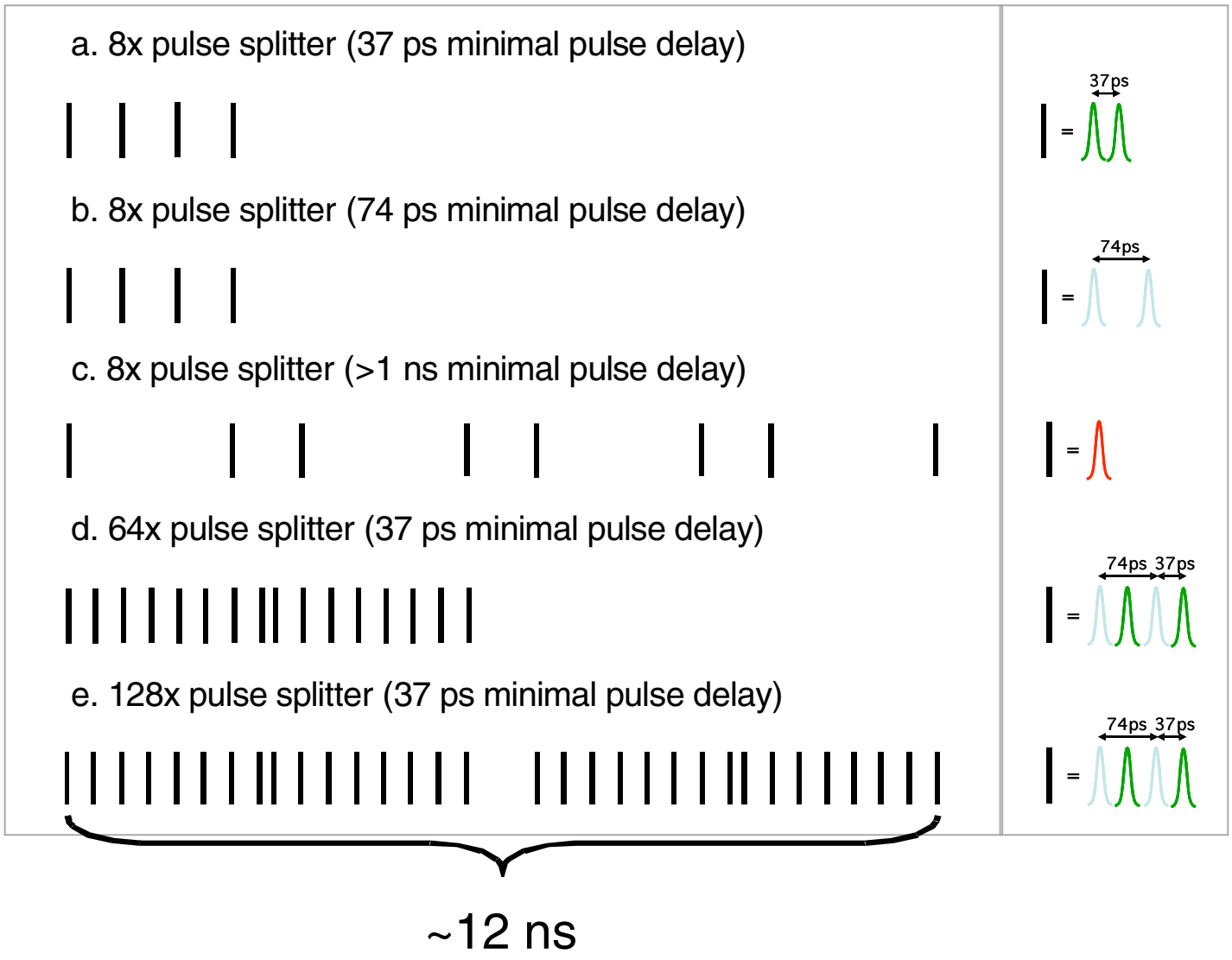

Supplementary Figure 4. Temporal sequences of pulse generated by each of the five splitter configurations in **Supplementary Fig. 3**: (a) 8x splitting, t = 37 ps; (b) 8x splitting, t = 74 ps; (c) 8x splitting, t > 1 ns; (d) 64x splitting, t = 37 ps; (e) 128x splitting, t = 37 ps.

Supplementary Figure 5 Unnormalized photobleaching curves of GFP-labeled *C. Elegans*

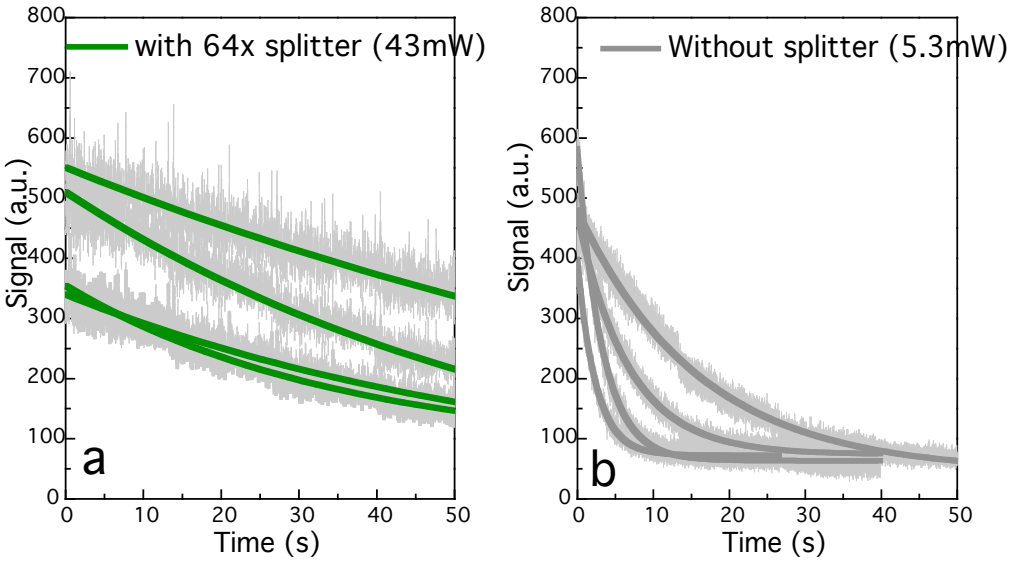

Supplementary Figure 5. The photobleaching curves in *C. Elegans* from **Fig. 4** of the main text, except before normalization, measured (a) with and (b) without a 64x pulse splitter. Note that the initial signals fall within the same range (300-600 a.u.) in the two cases.

Supplementary Figure 6 Ca^{2+} transient traces obtained with and without pulse splitting

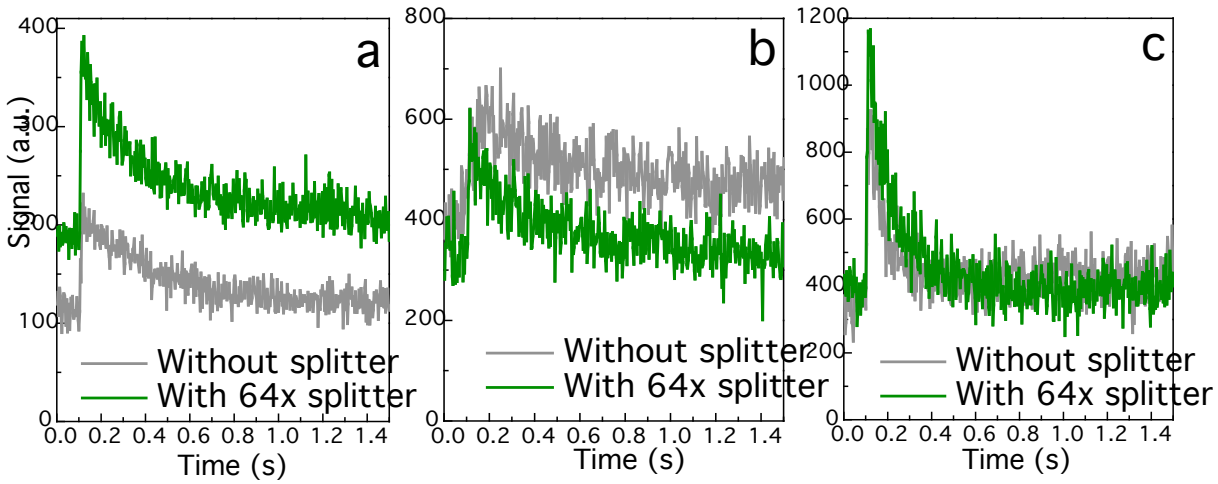

Supplementary Figure 6. Ca^{2+} transient traces at the beginning of each series of traces used to measure photodamage during Ca^{2+} functional imaging (**Fig. 5** in the main text). Average powers are: (a) 60 mW with 64x splitter, 5.7 mW without; (b) 66 mW with 64x splitter, 9 mW without; and (c) 100 mW with 64x splitter, 12.5 mW without. Note that considerably more signal was obtained in (a) with the splitter, due to the use of more than 8x higher average power.

Supplementary Methods

Preparation of fixed brain slices. C57Bl6 mice were injected with AAV2/1-GFP virus at postnatal day 13 to 15. Fourteen days later, animals were sacrificed and the brains were extracted. Brains fixed overnight in 4% paraformaldehyde were washed three times with phosphate buffer and then cut into 60 m thick sections using a vibratome (Leica, VT1000S). For long-term storage, such sections were mounted in Vectashield (Vevtor Laboratories).

Preparation of hippocampal brain slices. Transverse hippocampal slices (400 μm-thick) were prepared from 8 to 12-week old Sprague Dawley rats. Rats were given a lethal dose of ketamine and xylazine, perfused through the ascending aorta with an oxygenated solution just before death and decapitated. Hippocampal CA1 pyramidal cells were visualized using an Olympus BX-61 microscope equipped with differential interference contrast optics under infrared illumination. Experiments were performed at physiological temperature (34-36 °C) in ACSF containing the following (in mM): NaCl 125, KCl 3, $NaHCO_3$ 25, $NaHPO_4$ 1.25, $CaCl_2$ 1.3, $MgCl_2$ 1, and glucose 25; and was saturated with 95% O_2 and 5% CO_2. Current-clamp whole-cell recordings (somatic membrane voltage V_m= -65 mV) from somata were performed using a Dagan BVC-700 amplifier in the active 'bridge' mode, filtered at 3 kHz and digitized at 50 kHz. Patch pipettes had a resistance of 2-4 M when filled with a solution containing (in mM): K-methylsulphate 120, KCl 20, HEPES 10, NaCl 4, MgATP 4, Tris 2, GTP 0.3, phosphocreatine 14 (pH= 7.25). The series resistance was between 8-15 M . Neurons were filled with 200 μM Oregon green BAPTA-1 (OGB-1) (Molecular Probes, Eugene, OR, USA) and imaged with a TPE microscope using a water immersion lens (60X, 0.9 NA, Olympus, Melville, NY, USA). To ensure uniform filling and excitation of proximal dendrites access resistance was kept

minimal, a ten to fifteen minute filling time was given before recording were initiated. For the Ca^{2+} imaging experiments, two back-propagating action potentials were induced by somatic current injection (700 pA, 10 ms) at 6s intervals (0.17 Hz) and the Ca^{2+} transient in dendrites and spines was detected by rapid line scans (512 linescans at 333 Hz) using 830 nm excitation.

Preparation of GFP expressing *C. Elegans* Larvae. *C. Elegans* was grown on agar plates spread with *E. Coli* bacteria. Larvae were transferred onto 2% agarose gel, paralyzed by 50 mM 2,3-butanedione monoxime, and covered with a cover glass for imaging.

Pulse splitter design parameters. To form the upper region of the $t = 74$ ps and $t = 37$ ps pulse splitters used in this study (PS1 and PS2 respectively in **Fig. 1c** of the main text), two two-inch diameter fused silica plane parallel windows of thicknesses 0.5 inch (PS1, CVI Laser, PW1-2050-UV) and 0.25 inch (PS2, CVI Laser, PW1-2025-UV) were each custom-coated (Reynard Corp.) with a 50% reflective dielectric coating over the entirety of one face, and a >98% reflective coating over the center 0.6 inch (PS1) and 0.3 inch (PS2) diameter of the other. Both coatings exhibited constant reflectivity over the 780-910 nm wavelength range typical of TPE microscopy. Protected silver mirrors of diameter 0.5 inch (PS1, Thorlabs, PF05-03-P01) and 0.28 inch (PS2, Thorlabs, PF03-03-P01) provided the bottom reflective surfaces of the splitters. Precision ground spacers of thickness 0.28 inch (PS1) and 0.14 inch (PS2) were used to position each mirror with respect its corresponding window, thereby creating the air gap that served as the lower propagation medium within each splitter. With these gap dimensions, sub-pulses emerging from both output ports of each splitter were nominally spatially concentric at an input beam incident angle of 45 . In practice, each splitter was mounted on a rotational stage (Thorlabs, PR01) to optimize the overlap of all output beams.

To provide additional pulse splitting as in the configuration of **Fig. 1c** of the main text, non-polarizing beamsplitters divided (BS1, Thorlabs, BS011) and redirected (BS2, BS3, Thorlabs, BS011, BS017) the beams at various points, before a half-wave plate (HWP, CASIX, WPA1312-λ/2-700nm-1000nm) and polarizing beamsplitter (PBS, Newport, 10FC16PB.5) combined all beams into a common output. Pulse splitting on the longest time scale was accomplished with the aid of these beamsplitters and three identical 2.5 ns delay lines (DL), each consisting of opposed high-reflectivity (>99.8%) low-dispersion mirrors (Precision Photonics Corp, MI1000-TiD) separated by a 4.0 inch spacer. Pulses traveled three round trips between these mirrors before emerging. The whole pulse splitter setup is structurally stable. After an initial alignment, no re-alignment was needed over weeks of operation.

High-ratio pulse splitting. After N partial reflections at the interface between two media, one pulse is split into 2^N sub-pulses. However, for the splitter geometry shown in **Supplementary Fig. 1**, many of these sub-pulses overlap in time. If the reflectivity of the interface were 50% throughout, these overlapped pulses would behave as a single, more intense pulse relative to their non-overlapped neighbors. Achieving an optimal balance between signal and photodamage requires all pulses to have equal energy. The approach taken in **Supplementary Fig. 1** towards this end involves varying the reflectivity of the interface at each reflection point so that the overall energy of each temporally overlapped pulse is equivalent to that of those pulses that remain temporally distinct. In this case, N reflections of one input pulse at the interface lead to $2N$ output sub-pulses. The splitter shown in **Supplementary Fig. 1**, for example, generates 10 equal-energy output sub-pulses from one input pulse. Intermediate sub-pulses within the splitter are shown color-coded according to the medium they are in, arranged according to their temporal order, and drawn with heights proportional to their energy.

In the special case where pulse splitting ratios of 2^N will suffice, it is possible to create output sub-pulses of equal energy using N regions of 50% reflectivity, which split the pulse, and 2^{N-1}-N totally reflecting regions, which separate sub-pulses that would otherwise be temporally overlapped. For example, **Supplementary Fig. 2** depicts a 16x pulse splitter, where the reflectivity of the interface varies according to 50%, 50%, 100%, 50%, 100%, 100%, 100%, 50% at eight interfacial reflection points, from input to output. Requiring only two interfacial coatings of differing reflectivity considerably simplifies the fabrication of such splitters.

One factor limiting the pulse splitting ratio is group-delay dispersion (GDD) induced pulse broadening. It sets an upper limit on the distance L that a pulse may propagate through a dispersive material. When both input ports are used as in **Fig. 1b** of the main text, L is related to N, the number of output sub-pulses, and their separation t by:

$$N \cdot \Delta t = \frac{4L}{c}\left(\frac{n_1^2 - n_0^2}{n_1} \right).$$

The last sub-pulses in each output train face the greatest GDD (~2000 fs^2 for the 128x splitter) due to their longer path lengths within the dispersive portion of the device. However, autocorrelation measurements reveal that the optics in many microscopes contribute 4500 to 19000 fs^2 of GDD. Thus, an initial pulse of 140 fs width, typical of our laser, is expected to be broadened due to the inclusion of the 128x splitter by only an additional 9-15% beyond the effect of the microscope alone.

Calculation on the reduction of photobleaching by pulse splitting. Consider a nonlinear process of signal $S \propto I^{\alpha}$ and damage $D \propto I^{\beta}$, where $\beta > \alpha > 1$. The signal S_1 generated by one pulse will equal the signal S_N generated by an N-pulse splitter when

$I_1^{\alpha} = N(I_N)^{\alpha}$, or equivalently, $I_N = N^{-1/\alpha} I_1$, where I_1 and I_N are the respective pulse intensities. In this limit, the photodamage $D_N \propto N(I_N)^{\beta}$ with N pulses will be reduced to $N^{1-\beta/\alpha}$ times the damage D_1 with a single pulse. Of course, to obtain the same signal *rates* in the two cases, the N pulses must be delivered at N times the original repetition rate, requiring an average power at the sample greater by a factor of $N^{1-1/\alpha}$.